ELSEVIER

Contents lists available at ScienceDirect

Atmospheric Research

journal homepage: www.elsevier.com/locate/atmosres



Climatology of Sundowner winds in coastal Santa Barbara, California, based on 30 yr high resolution WRF downscaling



Charles Jones^{a,b,*}, Leila M.V. Carvalho^{a,b}, Gert-Jan Duine^b, Katelyn Zigner^a

- ^a Department of Geography, University of California, Santa Barbara, California, USA
- ^b Earth Research Institute, University of California, Santa Barbara, California, USA

ARTICLE INFO

Keywords:
Downslope windstorms
WRF
Sundowner winds
California
Santa Barbara
Wildfire hazards

ABSTRACT

Sundowner winds are a type of downslope windstorms observed on the southern slopes of the Santa Ynez Mountains (SYM) in Santa Barbara, southern California. The name "Sundowner" is due to the onset of strong winds near sunset. Sundowner winds can reach gale force and are extremely dangerous during wildfires. This study presents a climatology of Sundowners based on a 30 yr high spatiotemporal resolution dataset obtained with the Weather Research and Forecasting model. Combined empirical orthogonal function (EOF) analysis of hourly zonal and meridional winds (10 m) with 1 km grid spacing is performed to characterize the diurnal variability of surface winds. The first two eigenmodes (EOF-1, EOF-2) (58% of total variance) characterize the variability of surface winds in the western and eastern parts of the SYM, respectively. The hourly percentiles of the frequency distribution of the first two time coefficients (PC1, PC2) are used to identify three types of Sundowner regimes. The western (eastern) regime occurs when surface winds project strongly on EOF-1 (EOF-2) but not on EOF-2 (EOF-1). The western regime is characterized by a strong coastal jet around Point Conception with northwesterly winds extending into the Santa Barbara Channel. In contrast, a weak coastal jet not extending into the Santa Barbara Channel is observed in the eastern regime. In the Santa Barbara (SBA) regime, hourly surface winds project strongly on both EOF-1 and EOF-2. The western regime occurs more frequently than the eastern and SBA regimes and peaks during March-May. The eastern regime has maximum in January-February, whereas the SBA regime has a seasonal cycle similar to the western regime. Horizontal and vertical structures of winds and potential temperature show that the lee slope jet and mountain wave activity on the SYM exhibit strong spatial variations in the three regimes.

1. Introduction

Santa Barbara County in southern California (Fig. 1a) is characterized by unique geographic and climatic features. The cold Pacific Ocean and shallow marine boundary layer border a narrow coastal plain south of the Santa Ynez Mountains (SYM), which are narrow mountains stretching for about 100 km in the west-east direction with highest elevations between 1200 and 1435 m asl. The Santa Ynez Valley to the north of the SYM has a "V" shape approximately oriented from west to east with increasing elevations in its easternmost part. The San Rafael Mountains (SRM) (1800–2000 m asl) are the other dominant topographic features in the region.

The Mediterranean climate of southern California is often impacted by devastating wildfires that quickly spread to large sizes during extreme fire-weather conditions (i.e., high wind speeds, high temperatures, low humidity and dry vegetation fuels) (Kolden and Abatzoglou, 2018; Moritz et al., 2010). Under such conditions, the dominant atmospheric circulation feature in Ventura, Los Angeles and San Diego Counties is associated with Santa Ana winds. Santa Ana winds occur more frequently in late fall and winter and can reach "hurricane" force in the Santa Clara River Valley, Cajon and Banning Passes (Hughes and Hall, 2009; Jones et al., 2010; Raphael, 2003). In contrast, Sundowner winds have been studied much less and are a type of downslope windstorms with characteristics unique to Santa Barbara County (Carvalho et al., 2020; Hatchett et al., 2018; Ryan, 1996; Sukup, 2013). Sundowner winds (or Sundowners) are observed on the southern slopes of the SYM and typically initiate near sunset (thus, the origin of the name). Contrary to Santa Ana winds, Sundowners are observed year-round, with peak in frequency in spring (Hatchett et al., 2018). Sundowners have enhanced all major wildfires affecting Santa Barbara County, including the Thomas Fire in December 2017, the most devastating wildfire in recent history in Southern California (Kolden and Abatzoglou, 2018).

^{*} Corresponding author at: Department of Geography, University of 20 California, Santa Barbara, CA 93106, USA. *E-mail address:* cjones@eri.ucsb.edu (C. Jones).

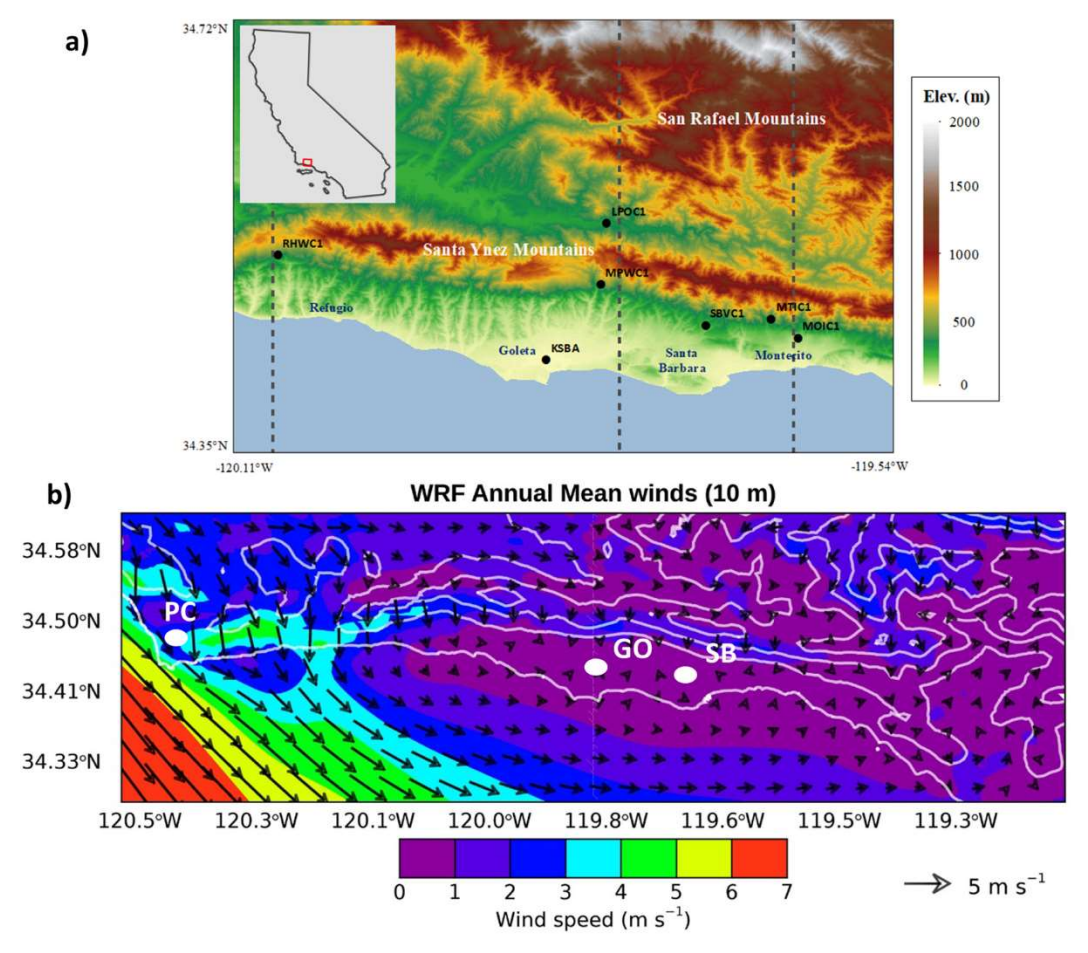


Fig. 1. a) Santa Barbara County topography (colors) and network of stations (dots) on the southern slopes of the Santa Ynez Mountains. The approximate location of urban centers (Goleta, Santa Barbara, and Montecito) and Refugio State beach are included. The inset map indicates the relative position of the domain in the state of California. Dashed lines are used in latitude versus height cross sections shown in Fig. 12 and referred to as "Refugio", "San Marcos" and "Montecito". b) annual mean climatology of WRF winds (10 m). Thin white contours show terrain elevations every 300 m. To increase clarity, wind vectors are plotted every 4th grid point. Locations of Point Conception (PO), Goleta (GO) and Santa Barbara (SB) are indicated by white circles.

Previous case studies have provided insights into the characteristics and potential mechanisms of Sundowner winds. Blier (1998) investigated synoptic conditions during three Sundowner cases distributed in different seasons and noticed significant mountain wave activity in the SYM and interactions of downslope winds with the marine boundary layer. Cannon et al. (2017) employed the Weather Research & Forecasting (WRF) model to analyze Sundowners and non-Sundowner conditions during case studies. They found that self-induced and mean-state critical layers associated with backing and reversal of winds in the lower troposphere appear to be relevant conditions to reflect gravity waves and accelerate winds on the slopes of the SYM. Duine et al. (2019) analyzed case studies and indicated that the extent of strong surface winds during Sundowners is sensitive to both planetary boundary layer and land-surface schemes used in WRF. The patterns of self-induced wave-breaking near mountain top and erosion of a stably marine boundary layer can be sensitive to numerical schemes in WRF.

While progress has been achieved in understanding Sundowner winds, the spatial inhomogeneity of surface weather stations and lack of upper air observations preclude an observational characterization of the vertical structure of mountain waves and interaction of surface winds with the marine boundary layer. To overcome this difficulty, Carvalho et al. (2020) discussed the Sundowner Wind Experiment-Pilot study (SWEX), in which 3 hourly radiosondes were launched from a single location to study a Sundowner wind event during 28–29 April 2018. They showed that Sundowner winds are associated with the

presence of a lee-slope jet, which appeared linked to mountain wave activity. The spatial variability of winds was also investigated with WRF simulations (1 km grid spacing) and surface observation. Their results showed that Sundowner winds exhibit large spatial variability on the slopes of the SYM and the onset of these winds are linked to the development of a lee-jet on the southern slopes of the SYM induced by enhanced mountain wave breaking near sunset.

The National Weather Service, Los Angeles/Oxnard Office (NWS LOX) identifies the occurrence of Sundowner winds when there is cross mountain flow with wind speeds exceeding 30 mph (13.4 m s⁻¹) and/ or gusts above 35 mph (15.6 m s⁻¹) on the southern slopes of the SYM. Based on years of experience in forecasting Sundowner winds, NWS LOX forecasters identified substantial case-to-case spatial variations in downslope windstorms along the SYM. This has prompted a differentiation between Gaviota and Montecito Sundowner wind events, which means that some events only occur in the western SYM, others only in the eastern part and others as a combination along the entire SYM. Recognizing this spatial variability, the NWS LOX uses mean sea level pressure differences among the Santa Barbara, Santa Maria and Bakersfield airports as metrics to forecast occurrences of Sundowner winds. Ryan (1996) and Sukup (2013) analyzed several historical cases and, consistent with the NWS LOX operational practice, confirmed the importance of mean sea level pressure gradients across the SYM and SRM as skillful metrics to monitor downslope windstorms activity.

Comprehensive studies about the climatology of winds in Santa Barbara are limited. While Hatchett et al. (2018) analyzed differences in synoptic circulations between Santa Ana and Sundowner winds based on data from a single weather station, the only climatological study of Sundowner winds to date is discussed in Smith et al. (2018a, 2018b). Those studies used WRF with 2 km grid spacing to produce an 11 yr dataset and develop an index to characterize the spatial and diurnal variability of downslope winds in the region. They argue that there is no distinct regime in Montecito (i.e., eastern SYM), but only a continuum of Sundowner winds based on wind direction at the ridge level of the SYM. In addition, they argue that the mean sea level pressure difference between Bakersfield and Santa Barbara airports, used by the NWS LOX, is not skillful in forecasting winds in the eastern SYM.

This paper presents a climatology of Sundowner winds based on a 30 yr high spatiotemporal resolution dataset obtained with the WRF model. This work differs substantially from the previous studies in terms of climatological record (30 yr versus 11 yr) and downscaling approach. In addition, the current study uses a different methodology to characterize the spatial variability of surface winds and, most importantly, objectively identifies three regimes of downslope windstorms in the SYM. In Section 2, the 30 yr regional model downscaling approach is described in detail. Section 3 presents a methodology to objectively identify significant downslope windstorms and Sundowner winds regimes. The climatological characteristics of Sundowners are presented in Section 4. Section 5 evaluates metrics of mean sea level pressure differences used by the NWS LOX. Section 6 discusses the results and conclusions.

2. High-resolution WRF downscaling

The Weather Research and Forecasting (WRF) model (Advanced Research WRF version 4.0.1) (Skamarock et al., 2008) was used to produce a 30 yr high-resolution downscaling climatology over Santa Barbara County. WRF was configured with 4 two-way nested grids with 27 km, 9 km, 3 km and 1 km horizontal grid spacings (Supplementary Material Fig. S1). This choice of grid spacing was motivated by two reasons. First, the 1 km grid resolves topographic features such as the SYM more accurately than 2 km grids. Cannon et al. (2017), for example, showed that simulations with 1 km compares slightly better with surface observations near the coast, which arises from a more accurately representation of land and ocean grid points near the coastline. Second, the 30 yr WRF dataset described here is being used as inputs to run uncoupled wildfire spread models and, therefore, surface winds accuracy is important for realistic wildfire simulations. The 1 km grid covers a large portion of southern California including the entire SYM and SRM (Fig. 1 b).

WRF was configured with 55 vertical levels and model top at 50 hPa. The configuration used numerical parameterizations for microphysics (Single moment 6-class, Hong and Lim, 2006), long-wave and short-wave radiation transfer (RRTMG, Iacono et al., 2008), Noah multi-parameterization options (Noah-MP) (Niu et al., 2011), surface layer physics and planetary boundary layer (MYNN, Nakanishi and Niino, 2009; Olson et al., 2019). This combination of parameterizations is similar to the one used in Duine et al. (2019), who performed extensive comparisons between WRF simulations and surface weather observations in the 1 km domain of analysis. Additional comparisons between WRF and seven weather stations were performed; these stations are shown in Fig. 1a and were selected based on the record of available observations (Supplementary Material Table S1). Temperature (2 m) model biases during MAM range from \pm 1.5C and root-mean square (rms) errors from 2-4C. Wind speeds (10 m) model biases range from \pm 3 m s⁻¹ and rms errors are 3 m s⁻¹ or less. Model biases in relative humidity (2 m) are ± 15% and rms errors of 15-20% (Supplementary Material Fig. S2). We note that the statistics vary appreciably among the stations, which is a result of model accuracy as well exposure problems frequently associated with some remote automatic weather stations (RAWS) (e.g., Cao and Fovell, 2016).

Initial and boundary conditions were obtained from the European Centre for Medium-Range Weather Forecasts Interim Reanalysis (ERA Interim) (Dee et al., 2011). WRF was initialized on 1 July 00UTC of a given year and integrated continuously until 1 September 00UTC of the following year and repeated for 30 yr. Sea surface temperature (SST) from ERA Interim was updated every 6 h. Grid nudging was applied in all model levels of the 27 km grid (nudging coefficient 0.0003 s⁻¹) so that WRF was forced to follow large-scale features from the reanalysis. The first two months of each integration were discarded to account for model spin up. The period of analysis is from 1 September 1987 to 31 August 2017 with model output saved every hour. This strategy was specifically chosen so that the model was initialized during the dry season and had enough time to adjust through the end of the wet season in southern California; the rainy season typically occurs during November-March in Santa Barbara County (Jones and Carvalho, 2012).

It is worth pointing out some differences in WRF downscaling approach done here and the study of Smith et al. (2018b). A detailed comparison is not possible, since the period of analysis and model initialization time are not specified in Smith et al. (2018b). Presumably, their 11-year climatology was done for the 2006-2016 period as suggested by Table 1 in Smith et al. (2018a). Smith et al. (2018b) used NCEP Global Forecast System (GFS) analyses as initial and boundary conditions. This study uses ERA Interim reanalysis, which has a fixed data assimilation system and forecast model and, therefore, large-scale atmospheric fields are consistently derived over time. Smith et al. (2018b) performed their 11-year climatology by running month-long simulations and disregarding model spinup. This study discards 2 months of model spinup and analyzes 12-month long simulations. Lastly, SST update is important in 1-month or longer high-resolution WRF simulations because SST gradients in the Santa Barbara Channel can be significant and influence land-ocean circulations (Cannon et al., 2017). While SST was updated once a month (before 2013) and daily (after 2013) in Smith et al. (2018b), the current study employed 6 h SST updates throughout the 30-year WRF simulations.

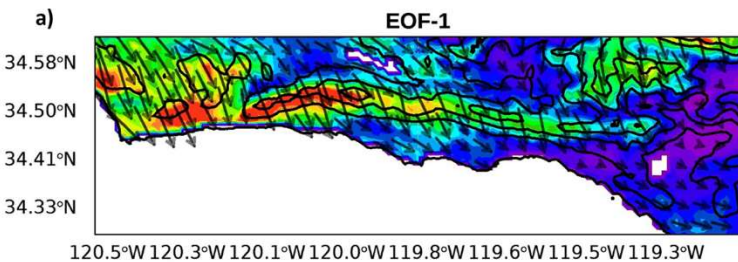
3. Combined empirical orthogonal function analysis

Fig. 1b shows the annual mean climatology of WRF simulated winds (10 m). A clear east-west gradient in winds is evident with maximum winds found off the coast near Point Conception and low elevations of the western SYM. The climatology, variability and mechanisms of the strong ocean surface winds, known as coastal jet, has been extensively investigated (Dorman and Koračin, 2008; Doubler et al., 2015). While annual mean winds are weak over land, it is also noticeable that speeds are stronger on the SYM slopes than over the coastal plain. As it will be demonstrated later, downslope winds on the southern slopes of the SYM can be much stronger than the mean winds. To characterize the diurnal variability of surface winds and objectively identify strong downslope winds, we have applied combined empirical orthogonal function (CEOF) analysis (Wilks, 2011). The reader is referred to Ludwig et al. (2004) for additional discussions on EOF analysis and application to wind datasets and Conil and Hall (2006) for regional model characterization of Santa Ana winds.

Since the amount of data is very high, a sub-domain of the WRF 1 km grid was chosen. First, the long-term mean (Fig. 1b) was subtracted from the hourly zonal (u10) and meridional (v10) winds (10 m). Next, eigenvalues and eigenvectors were computed from a covariance matrix (6566 \times 6566 points) constructed with hourly u10 and v10 data from 1 Sep 1987 to 31 Aug 2017. Only grid points over land were included in the calculation. This procedure was designed to emphasize winds over the SYM and SRM and avoid large loadings associated with the coastal jet. The first five eigenvalues explain 34.9%, 23.1%, 5.0%, 3.8% and 2.8% of the total variance, respectively. The first two eigenvalues are separated from the remaining ones according to the North et al. (1982) criterion. The results are qualitatively similar if one includes ocean and land grid points, but the procedure above was

b)

34.58°N 34.50°N 34.41°N 34.33°N



12

Wind speed (m s⁻¹)

16

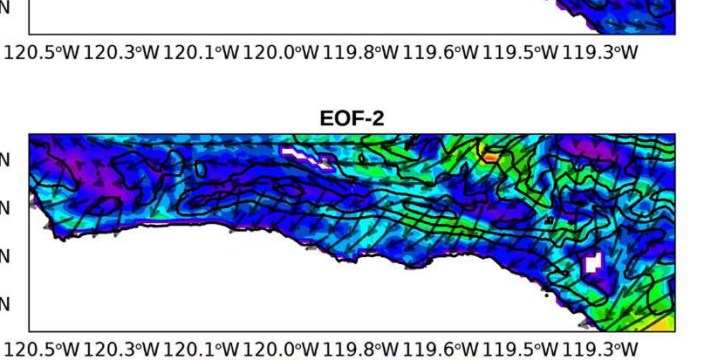


Fig. 2. a) First combined empirical orthogonal function pattern (EOF-1) of winds at 10 m above ground level. b) same as on top, but for second combined empirical orthogonal function pattern (EOF-2). Colors indicate wind speeds (m s $^{-1}$) and thin black contours show terrain elevations every 300 m. EOF patterns have been scaled by the square root of the corresponding eigenvalues. To increase clarity, wind vectors are plotted every 4th grid point.

deemed optimal to identify Sundowners.

The first eigenvector (EOF-1) (Fig. 2a) captures a substantial part of the surface wind variability with largest loadings in the western half of the domain. Additionally, large loadings are observed over the southern slopes of the eastern SYM and SRM. In contrast, the second eigenvector (EOF-2) (Fig. 2b) represents a different spatial pattern with large loadings on the southern slopes of the SYM in Santa Barbara (119.7 W-119.5 W) and to the north over the SRM. Previous studies discuss the existence of two regimes, in which Sundowner winds are observed over the western or eastern SYM (Cannon et al., 2017; Carvalho et al., 2020; Sukup, 2013). The western regime identified in this study has some similarities to what Smith et al. (2018a, 2018b) call "Gaviota type" of Sundowner winds, whereas the eastern and SBA regimes identified here were not identified in those studies. The CEOF method distinctively characterizes such variability along the entire SYM with EOF-1 representing the western and EOF-2 characterizing the eastern variability of downslope winds.

Additional analysis (not shown) indicate that the first time-coefficient (PC1) leads the second time-coefficient (PC2) by about 6 h (correlation of 0.32, statistically significant at 5% confidence level). EOF-1/ PC1 and EOF-2/PC2 represent 58% of the total variance of surface winds. We employ these two eigenmodes to characterize diurnal and seasonal variability of downslope winds along the SYM. The hourly frequency distribution of PC1 (Fig. 3a) shows a clear diurnal cycle with positive values representing downslope winds along the SYM from midafternoon through the night; the maximum occurs at 17-18 PST. The hourly distribution of PC2 (Fig. 3b) shows a diurnal variation shifted in time relative to PC1 with median values maximized during 23-02 PST. Using the observational fact that Sundowner winds are associated with strong downslope winds starting in late afternoon (Blier, 1998; Carvalho et al., 2020; Sukup, 2013), maximizing during the night and ceasing in early morning, extreme values of the hourly frequency distributions of PC1 and PC2 were used to identify Sundowner winds. The western regime occurs when surface winds project strongly on EOF-1 but not on EOF-2. Conversely, surface winds project strongly on EOF-2 but not on EOF-1 in the eastern regime. Additionally, when surface winds project strongly on both EOF-1 and EOF-2, downslope winds are observed along the entire SYM (hereafter referred to as Santa Barbara regime, or SBA). Thus, these three types of Sundowner wind regimes are defined here according to the following criteria:

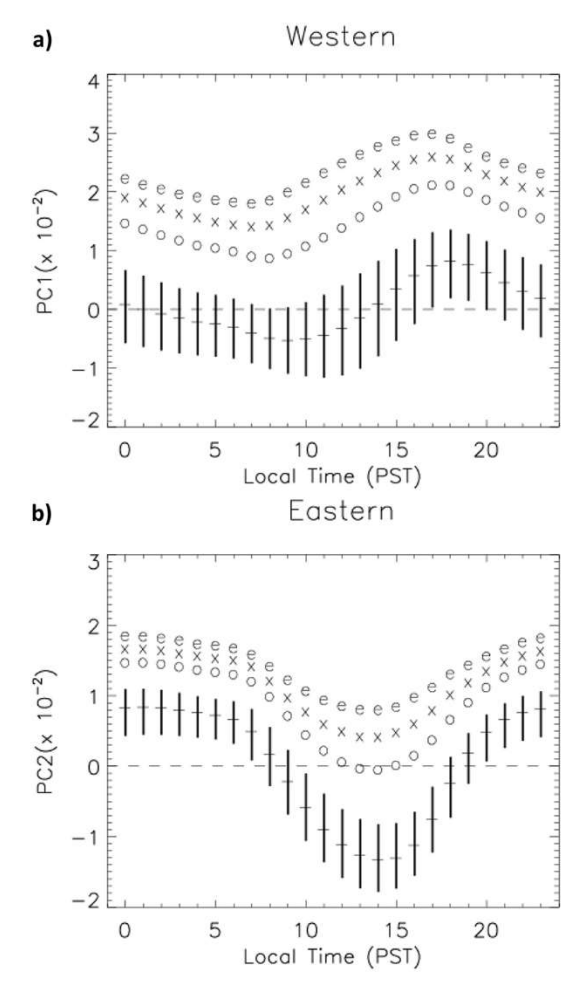


Fig. 3. a) Hourly frequency distributions of the first (PC1) time coefficient. b) Hourly frequency distributions of the second (PC2) time coefficient. Vertical bars indicate inter-quartile range with median value indicated by the tick mark. Percentiles of 90th, 95th and 97.5th are indicated by "o", "x" and "e" symbols. Horizontal axes indicate local time. Distributions are calculated from hourly data from 1 Sep 1987 to 31 Aug 2017 (262,992 data points).

- I. Western Regime: the hourly value of PC1 exceeds the 90th percentile from 16 to 7 PST, 2) the hourly value of PC2 does not exceed the 95th percentile from 20 to 7 PST and 3) the event lasts at least two consecutive hours.
- II. Eastern Regime: the hourly value of PC1 does not exceed the 90th percentile from 16 to 7 PST, 2), the hourly value of PC2 exceeds the 95th percentile from 20 to 7 PST and 3) the event lasts at least two consecutive hours.
- III. Santa Barbara Regime: the hourly value of PC1 exceeds the 90th percentile from 16 to 7 PST and the hourly value of PC2 exceeds the 95th percentile from 20 to 7 PST and 2) the event lasts at least two consecutive hours.

Each day in the period of analysis was tagged as a Sundowner or non-Sundowner day. The first hour of the Sundowner event was used to tag the occurrence of a Sundowner day. The total number of days in each category were 1341 (western), 556 (eastern) and 304 (SBA). Here, we are specifically interested in characterizing downslope winds that represent critical conditions for fast wildfire spread toward coastal Santa Barbara. Thus, percentile thresholds (conditions I-III) were tested by comparing cases selected by the algorithm with known Sundowner winds observed in Santa Barbara County. Supplementary material Table S2 shows Sundowner winds during some major wildfires as well as Sundowner events without wildfires studied in previous publications. It also includes the average values of PC1 (16–7 PST) and PC2 (20–7 PST) and percentile values which were exceeded in the corresponding time intervals.

4. Sundowner winds characteristics

4.1. Frequency

Hourly occurrences of the three Sundowner wind regimes were identified using the entire 30 yr WRF dataset (00UTC 1 September 1987 to 23 UTC 31 August 2017). Fig. 4a shows the monthly frequency distribution of each regime. The western regime has the highest frequency throughout the year, maximizes in spring (28%) and shows a secondary peak in Dec (12.2%). The eastern regime maximizes during Jan-Feb (8–9%), minimizes in summer and increases again in late fall (8%). Interestingly, the frequency of SBA regime has only one maximum in Apr (8%), which is actually higher than the eastern regime. The frequency of western regime agrees with Smith et al. (2018a, 2018b) and Hatchett et al. (2018) who reported maximum frequency in Apr-May. The persistence of each regime (Fig. 4b) indicates that most events last 1–3 days, although extreme western regime cases can last longer than 4 days. Cannon et al. (2017), for example, analyzed a case study that lasted 11 days (see also Supplementary material Table S2).

4.2. Synoptic characteristics

Fig. 5 shows composites of mean sea level pressure (mslp) and geopotential height at 500 hPa associated with each regime as well as non-Sundowner winds during spring; the season with the highest frequency of Sundowners. Sundowner winds in all regimes are associated with enhanced North Pacific subtropical High pressure and geopotential height (500 hPa) relative to non-Sundowner winds. Furthermore, distinct mslp gradients in southern California characterize each regime. In the western regime (Fig. 5a), a trough is present over the western U.S. and surface low pressure centers are located over the Great Basin and northern Mexico; mslp differences of 2-4 hPa between the south end of the state and the coast are observed. This synoptic pattern during the western regime seems also consistent with the Sundowner events discussed in Hatchett et al. (2018) (see their Fig. 3j) and Carvalho et al. (2020) (see their Fig. 3). In contrast, in the eastern regime (Fig. 5b), the surface low pressure is displaced to northern Mexico, the center of the North Pacific subtropical High exceeds 1024 hPa and approaches the west coast of the US. Notice also that the 500 hPa trough is displaced farther east over the Great Basin. For comparison, the synoptic pattern of the case study analyzed in Cannon et al. (2017) closely resembles Fig. 5b (see also Supplementary material Table S2). The synoptic pattern during the SBA regime (Fig. 5c) is a combination of both western and eastern regimes. The North Pacific subtropical High is stronger in the SBA regime (observe the 1026 h-Pa isobar) and exhibits a spatial pattern over the ocean and west coast that resembles the eastern regime. A strong mslp gradient is observed along the southern California coast. During non-Sundowner winds (Fig. 5d), the North Pacific subtropical High is zonally elongated and mslp gradients in southern California are much smaller than during Sundowners.

4.3. Spatiotemporal variability of surface winds

The spatiotemporal variability of Sundowner winds is now discussed in detail. Fig. 6 shows diurnal variations in surface winds (10 m) in the three regimes during MAM. The plots are computed as differences between composites of wind speeds in the regime minus non-Sundowner winds and displayed along the 300 m elevation on the southern slopes of the SYM. Note that SYM elevations west of 120.2 W are lower than 300 m and, therefore, the panels have constant wind speed differences. The number of cases in the western, eastern and SBA regimes are 688, 152 and 185, respectively. In the western regime (Fig. 6a), the onset of strong downslope winds (\geq 6 m s⁻¹ non-Sundowner wind speeds) in the western SYM (120.2-120.0 W) occurs near 16-17 PST. The onset of Sundowner winds along 120 W-119.5 W occurs 1-2 h later than in the western SYM, suggesting a delay in the onset of downslope winds in the eastern SYM. This feature has been discussed in Cannon et al. (2017) case studies. In contrast, in the eastern regime (Fig. 6b), although surface winds are strong in the western SYM, downslope winds are much stronger than the climatology in the eastern SYM. In the SBA regime (Fig. 6c), the diurnal variability during the SBA regime shows much less contrasts between the western and eastern SYM. The demise of Sundowner winds is quite variable along the SYM tending to occur between 6 and 8 PST and large spatial variability of downslope winds is noted.

The spatial variability of Sundowner winds is further demonstrated with composites of surface winds. In the western regime (Fig. 7), an enhanced coastal jet (speeds $\geq 12 \text{ m s}^{-1}$) is observed near the onset of Sundowner winds (16 PST). Additionally, downslope winds in the western SYM increase from 7 m s⁻¹ (16 PST) to over 10 m s⁻¹ during the night (19-23 PST) propagating eastward along the SYM. Subsequently, downslope winds and the coastal jet decrease in intensity (2 PST). It is also worth noting that strong north-northwesterly winds extend from Point Conception to the eastern Santa Barbara Channel, likely a result of the mslp gradient in southern California (Fig. 5a), which forces northwesterly winds in western SYM. During the western regime, downslope winds in the SRM are moderate ($\cong 7-9 \text{ m s}^{-1}$) at night (23-2 PST). The spatial patterns at 16 PST and 19 PST appear consistent with Smith et al. (2018a), particularly the enhanced coastal jet and strong northwesterly winds in the Santa Barbara Channel. Smith et al. (2018a) argue that the strength of the coastal jet is the primary control of Sundowner winds.

A different spatial pattern is observed during the eastern regime (Fig. 8). The coastal jet is significantly less intense (< 10 m s $^{-1}$) and, most importantly, intense northwesterly winds do not extend eastward along the Santa Barbara Channel throughout the day, a distinct difference from the western regime. This is likely related to the nearly northwest-southeast orientation of mslp gradient in southern California (Fig. 5b), which forces northerly to northeasterly winds in the SYM. While downslope winds occur in the western SYM between 16 and 23 PST, Sundowner winds are especially strong on the foothills of the cities of Goleta and Santa Barbara from 19 PST to 2 PST. Another important feature is the corresponding increase in downslope winds in the SRM, suggesting that both mesoscale circulations are likely related.

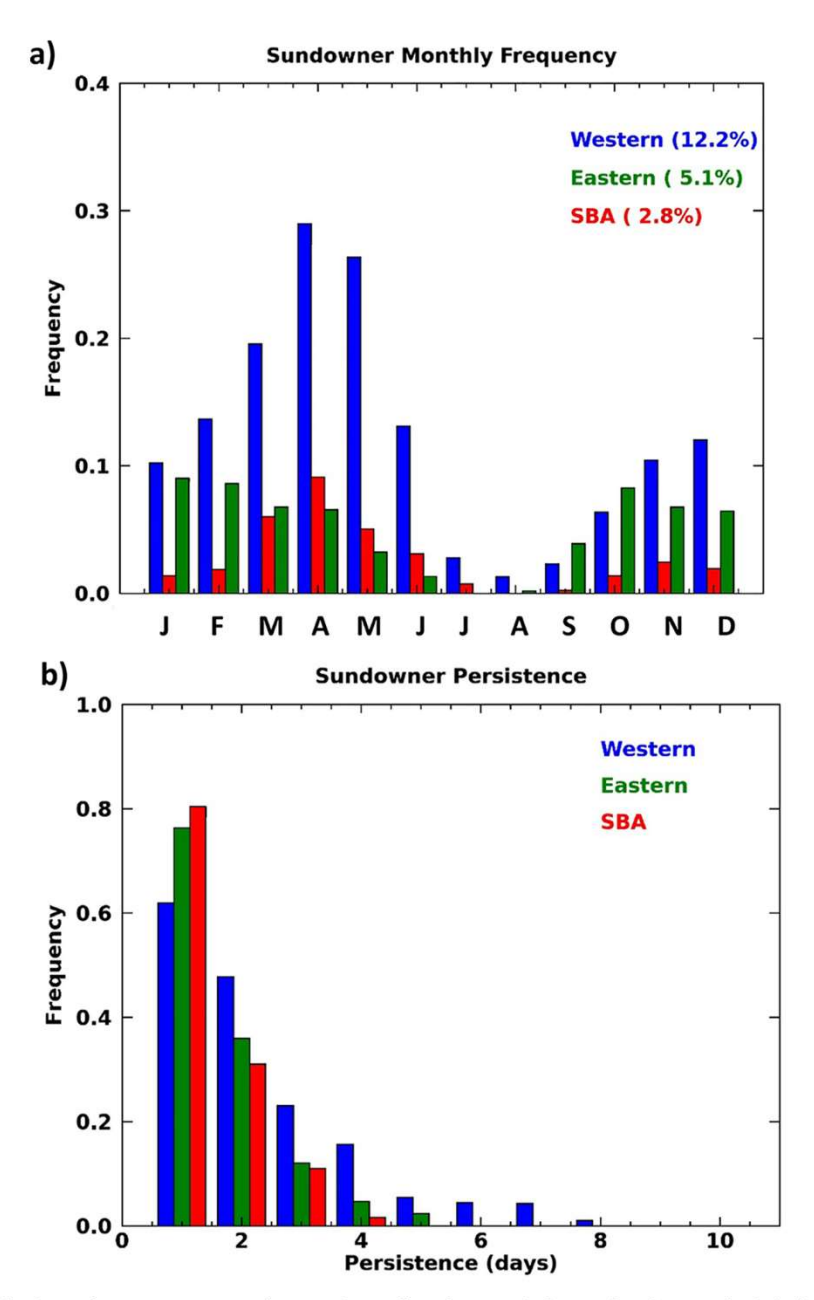


Fig. 4. a) Monthly frequency distributions of western, eastern and SBA regimes of Sundowner winds. Numbers in parenthesis indicate the percentage of days in each regime. b) Persistence of Sundowner wind days in each regime (see text for additional details).

The SBA regime (Fig. 9) shows a distinct spatial pattern from the western and eastern regimes, indicating remarkably strong winds along the slopes and foothills of the SYM during 19–23 PST. The coastal jet exceeds $\geq 14~{\rm m~s}^{-1}$ and extends to the eastern Santa Barbara Channel during 16–23 PST. Moreover, Sundowner winds are observed over the entire SYM during 19–23 PST and downslope winds exceed 14 m s $^{-1}$ over the SRM, which is one of the main differences from the western regime. A west-to-east progression of the strongest winds is observed from sunset to early morning.

To demonstrate the difference between the western and SBA regimes, Supplementary Material Fig. S3a shows the difference in WRF wind speeds (10 m) between the two regimes for each time shown in the composites in Figs. 7 and 9. At 16 PST, wind speed differences are on the order of 2 m s $^{-1}$ or less in the western and eastern SYM, but they start to increase by 19 PST. At 23 PST, wind speeds are about 5–7 m s $^{-1}$ stronger in the eastern SYM and SRM (119.7 W-119.5 W) in the SBA regime than in the western regime. Conversely, winds are 3–4 m s $^{-1}$

stronger in the western SYM in the western regime than in the eastern regime. At 2 PST, wind speeds are even stronger near Montecito $(7~{\rm m~s^{-1}})$. Supplementary Material Fig. S4 shows that standard deviations of WRF winds are about 1.5–3.5 m s $^{-1}$ in most locations and a little higher in the western SYM. Considering that rms errors between WRF simulated winds and surface stations are about 3 m s $^{-1}$, these results show that the magnitudes of the wind speed differences between the western and SBA regimes are above model uncertainty.

Supplementary Material Fig. S5 shows statistically significant (5% level) differences in mslp between the SBA and western regimes. It shows that mslp is more than 3 hPa higher in the SBA than in the western regime over a large area in the western U.S. Most importantly, mslp differences (\sim 1 hPa) extend to southern California and the Sundowner winds domain of study. Taken together, these results support the existence of three separate Sundowner wind regimes.

While composites describe average behavior, it is illustrative to show individual cases to highlight differences between the western and

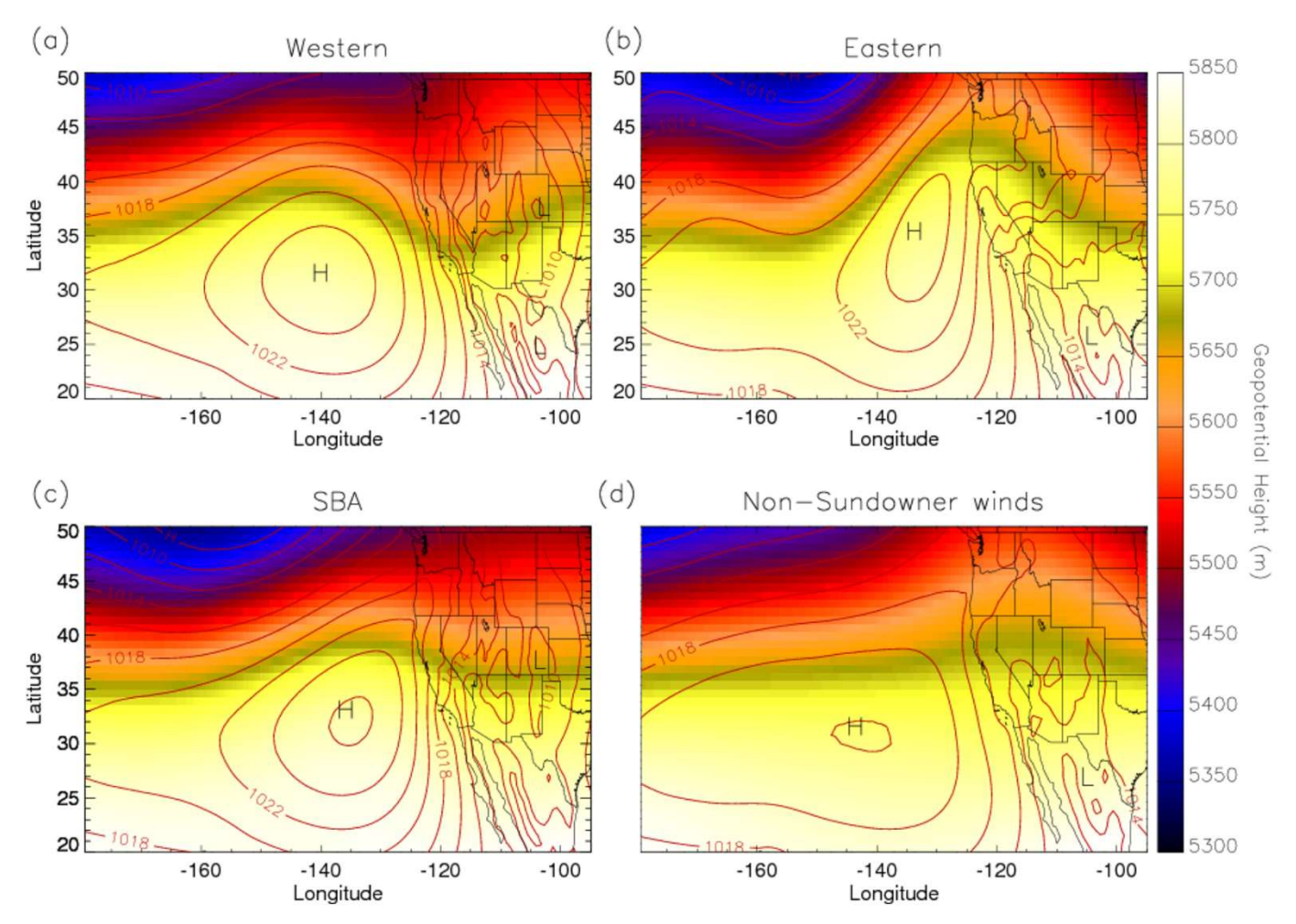


Fig. 5. Composites of Sundowner wind events during (a) western (688 events), (b) eastern (152 events) and (c) Santa Barbara (SBA) (185 cases) regimes; (d) composite during non-Sundowner winds (1735 cases). Color shading shows geopotential height at 500 hPa; contours show mean sea level pressure with 2 hPa interval. Season: 1 March- 31 May 1988–2017.

eastern regimes. However, as discussed earlier, a major challenge to characterize the spatial variability of Sundowners is the lack of a dense network of surface observations. The Montecito (MTIC1) station (498 m elevation) has a long record of observations and is situated in the eastern SYM; the Refugio (RHWC1) station (443 m elevation) is the westernmost station in the SYM with available observations coinciding with only two years of the WRF downscaling. To emphasize climate differences between the two stations, we note the distinct magnitudes of the 95th percentiles of surface winds during MAM: 7 m s $^{-1}$ MTIC1 and 13.5 m s $^{-1}$ RHWC1.

Fig. 10 shows a western Sundowner case that happened on 26 March 2017. Fig. 10a, b shows hourly surface winds in MTIC1 and RHWC1 as well as WRF simulated winds. Winds in Refugio already peaked at 10 m s⁻¹ at 15 PST, increased to stronger magnitudes in late afternoon and persisted until the next morning. In contrast, sustained winds in Montecito barely exceeded 5 m s⁻¹ (gusts of \sim 10 m s⁻¹) and did not meet the NWS LOX criteria of Sundowner winds. The diurnal variability of WRF winds closely followed the observed sustained winds in Refugio, while WRF overestimated sustained winds in the Montecito station. It is worth pointing out that the Montecito station is located downslope of a small canyon and is more exposed to strong northerly winds; in this western regime case, sustained winds at station were less than 6 m s⁻¹ during 15:47 09:47 PST. The WRF simulation on 26 March 2017 at 22 PST (Fig. 10c) clearly showed much stronger winds in the western than eastern SYM. Notice also the strong coastal jet and strong northwesterly winds in the Santa Barbara Channel. The projection of surface winds onto EOF-1 was large and PC-1 exceeded the PCs thresholds previously discussed.

Fig. 11 shows an eastern regime case on 11-12 March 2017, also discussed in Duine et al. (2019). The Montecito station (Fig. 11a) showed rapid increases in surface winds in late afternoon that exceeded 15 m s⁻¹ during the evening and night. Winds in Refugio were also strong (Fig. 11b) and above 10 m s⁻¹, although weaker than in Montecito. The diurnal variability of WRF simulated winds agrees quite well with sustained winds at MTIC1; as mentioned previously, that station is more exposed to strong northerly winds. Over the western SYM, WRF simulated wind speeds above 10 m s⁻¹ displaced westward of the maximum winds and at lower elevations as typically occurring during the western regimes. Consequently, WRF underestimated winds in RHWC1 (see red box, Fig. 11), which is located slightly east of the strongest winds, by as much as 10 m s⁻¹ in late evening. Despite the fact that WRF underestimated winds near RHWC1, the projection of WRF winds onto to the EOFs classifies this event in the eastern regime. This is clearly shown in the WRF simulation (Fig. 11c), which indicates very strong northeasterly surface winds in the eastern SYM and SRM. This pattern is spatially correlated with the corresponding composite (Fig. 8). Additionally, note that the coastal jet was significantly weaker than in the western case (compare Fig. 10c, 11c) and strong northwesterly winds in the Santa Barbara Channel were absent.

Supplementary Material Fig. S6. shows an event on 13–14 April 2017 classified as SBA regime. WRF simulated winds agree reasonably well with the diurnal variation of sustained winds in MTCI1 and

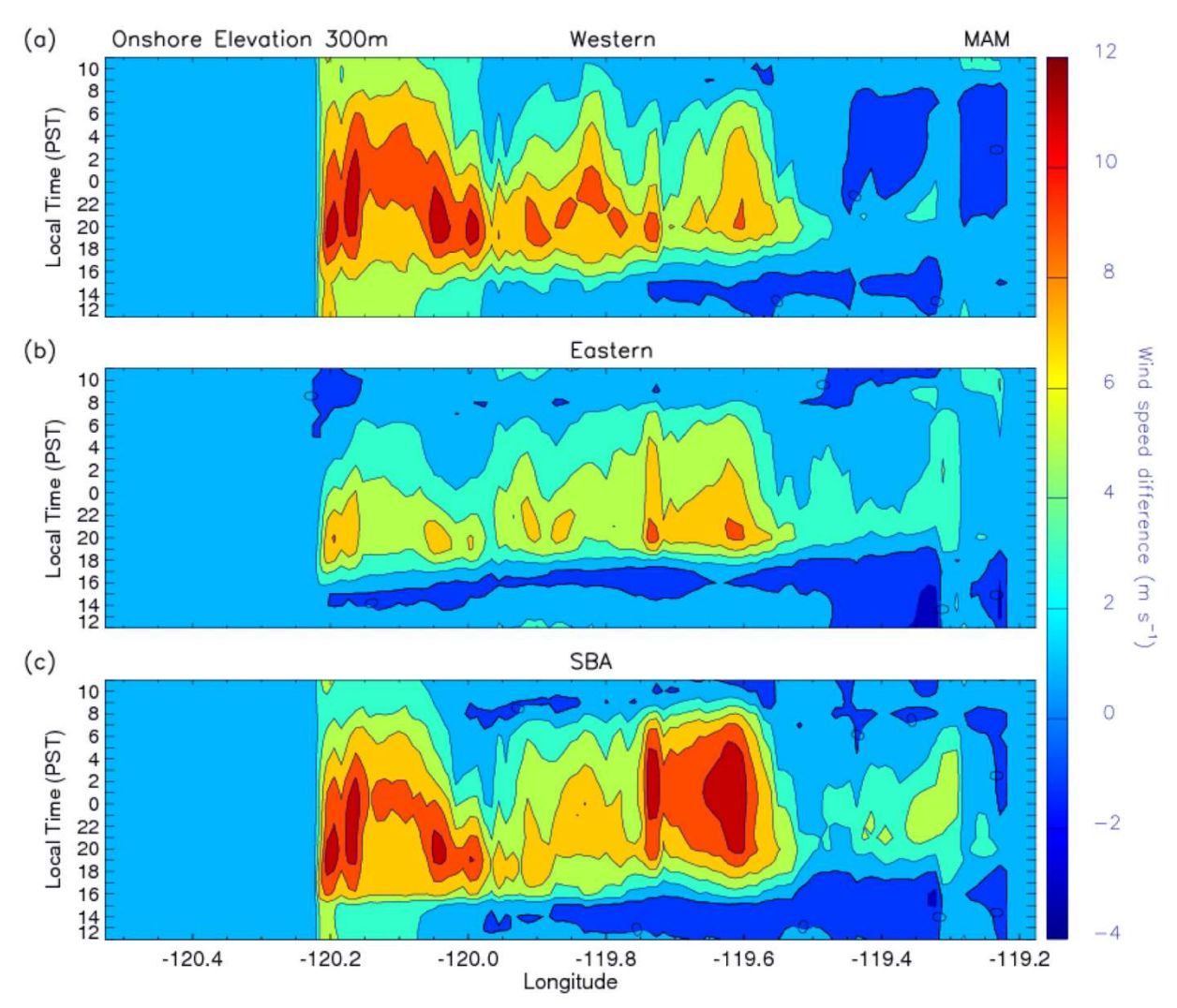


Fig. 6. Diurnal variations of wind speeds during MAM of a) western, b) eastern and c) SBA regimes. Plots show wind speed (m s⁻¹) differences from non-Sundowner wind days along the 300 m elevation on the southern slopes of the Santa Ynez Mountains. Ordinate axes are in local time (PST). Note that terrain elevations westward of 120.2 W along the coast do not exceed 300 m and wind speeds are constant.

RHWC1, although WRF underestimates the peak magnitudes. WRF simulated winds clearly shows strong downslope winds along the entire SYM, strong downslope winds over the SRM, strong coastal jet and strong northwesterly winds in the Santa Barbara Channel.

In summary, the magnitude of the projection of WRF surface winds onto the EOFs are used to classify strong downslope winds according to western, eastern and SBA regimes. It is important to realize that when downslope winds in the eastern SYM are strong in the eastern regime, downslope winds in the western SYM can still be large especially westward of Refugio (inclusive). The lack of a dense network of surface meteorological stations underscores the challenge of accurately simulating surface winds and point out model improvements needs.

4.4. Vertical structure

Fig. 12 shows composites of vertical cross sections of potential temperature and meridional winds along three longitudes (Refugio, Santa Barbara County Fire Department Headquarters, SBCFD HQ, and Montecito; see also Fig. 1a) during western, eastern and SBA regimes at 19 PST and 23 PST. The longitude along "San Marcos" is shown because it aligns approximately with the San Marcos Pass and is the location studied during the Sundowner wind event discussed in Carvalho et al. (2020). At 19 PST and 23 PST in the western regime, intense mountain wave activity is noticed on the SYM with the lee slope jet reaching

meridional downslope (southerly) wind speeds exceeding 14 m s⁻¹ (Fig. 12 a-f). In this regime, the depth of the lee slope jet decreases from Refugio to Montecito and surface winds are not strong over low elevations. A markedly different pattern is observed during the eastern regime (Fig. 12 g-l). While the lee slope jet is strong in Refugio and San Marcos at 19 PST, it weakens in both locations at 23 PST. In contrast, meridional winds in Montecito remain less than -10 m s^{-1} . Furthermore, southerly winds greater than 2 m s⁻¹ are observed over a deep layer above the northerly winds, particularly over San Marcos and Montecito at 23 PST (Fig. 12 l) indicating directional wind shear above mountain top and presence of critical layers (Durran, 1990). Similar patterns have been observed in a case study discussed by Cannon et al. (2017). A comparison between Fig. 12 a-f and 12g-l show that the lower troposphere is warmer in the eastern than in the western regime. Consistent with the results shown earlier, strong northerly winds are noted in the SBA regime along the cross sections (Fig. 12 m-r). Interestingly, however, that the SBA regime is not a simple combination of the western and eastern regimes; a key difference is the profiles of stability and winds above 1500 m. It is also important to note that there are considerable horizontal and vertical variations from case-to-case, which are smoothed in the composites. Carvalho et al. (2020) discusses the vertical structure of Sundowner winds observed with radiosonde observations and model simulations during one case study that resembles the western regime discussed here.

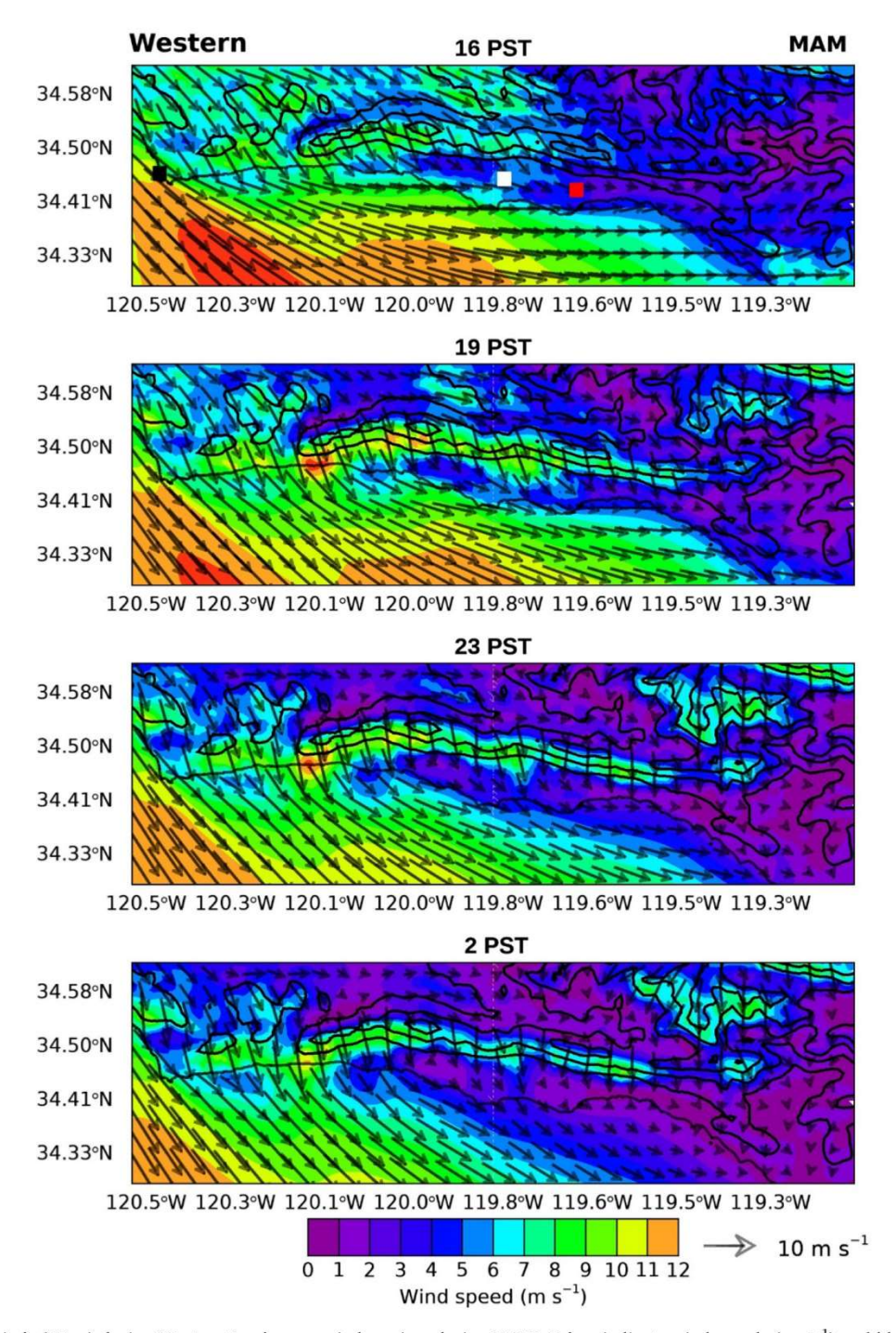


Fig. 7. Composites of winds (10 m) during Western Sundowner winds regime during MAM. Colors indicate wind speeds (m $\rm s^{-1}$) and black contours show terrain elevations every 300 m. Local times (PST) are indicated on top of each panel. Black, white and red squares indicate Point Conception, Goleta and Santa Barbara locations.

The cross-sections (Fig. 12) show that potential temperatures on the southern slopes of the SYM and low elevations in the Santa Barbara coastal plain originate from elevations above mountain top, as expected from downslope mountain waves (Durran, 1990). Carvalho et al. (2020) showed that air parcels reaching the foothills of the SYM during a Sundowner event have originated at pressure levels below 700 hPa during evening hours. To gain a better understanding about the extent to which mountain waves influence the atmosphere on the southern slopes of the SYM and coastal plain during Sundowner winds, we investigated variations in near ground level isentropes. Fig. 13 shows composites of potential temperature (2 m, θ_{2m}) and winds (10 m) in the

evening (20 PST). Several interesting aspects can be observed in these composites. Overall, the western regime is associated with cooler conditions compared with the other two regimes. Nonetheless, the θ_{2m} isentropes show important communalities: they clearly indicate the influence of mountain waves transporting air from above mountain top to the slopes and coastal SB and the extent of this transport (Fig. 13). They also indicate the importance of topography with generally warmer θ_{2m} downhill of the highest elevations. For instance, in the western regime (Fig. 13 a), θ_{2m} on the SYM slopes and coastal plain (\cong 292.5 K) are higher than offshore (\cong 286 K). θ_{2m} over the SYM slopes and coastal plain are warmer in the eastern (Fig. 13b) than in the western regimes;

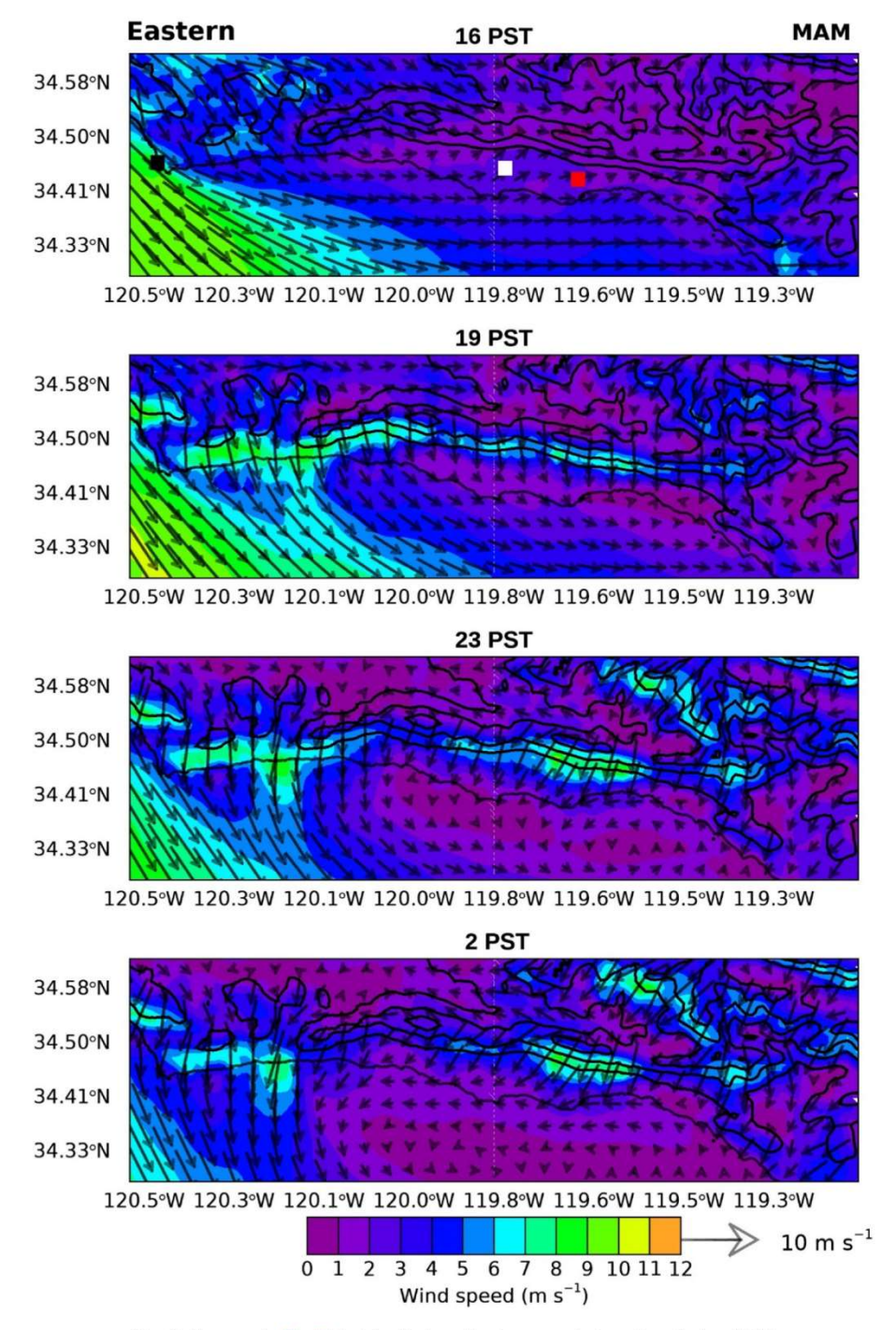


Fig. 8. Same as in Fig. 7, but for Eastern Sundowner winds regime during MAM.

differences on the order of 4–7 K are observed between the coastal plain and offshore. The spatial pattern of potential temperatures (2 m) in the SBA regime (Fig. 13c) has features from the western and eastern regimes. An important feature to note is the large east-west variability in warming on the southern slopes of the SYM and coastal plain (\cong 3–6 K) demonstrating the complex localized nature of Sundowner winds. This aspect shows that large skewness is introduced in indexes that spatially average winds and temperatures from Point Conception eastward toward Montecito as proposed by Smith et al. (2018a, 2018b).

Sundowners are often associated with increases in surface temperature and decrease in relative humidity during the onset of strong

downslope winds (Cannon et al., 2017; Carvalho et al., 2020; Sukup, 2013). Fig. 14 shows the frequency of days in the western (a) and eastern (b) regimes when relative humidity (2 m) is less than 20% at 20 PST. The effect in relative humidity is clearly noted on the southern slopes of the SYM and coastal plain. In the western regime, decreases in nighttime relative humidity are 7-14% of days, whereas in the eastern regime the frequency is > 65%. While the frequency of Sundowner winds in the eastern regime is less than in the western regime (Fig. 4), characterizing and forecasting these events is of critical importance to increase resilience to major wildfires in Santa Barbara.

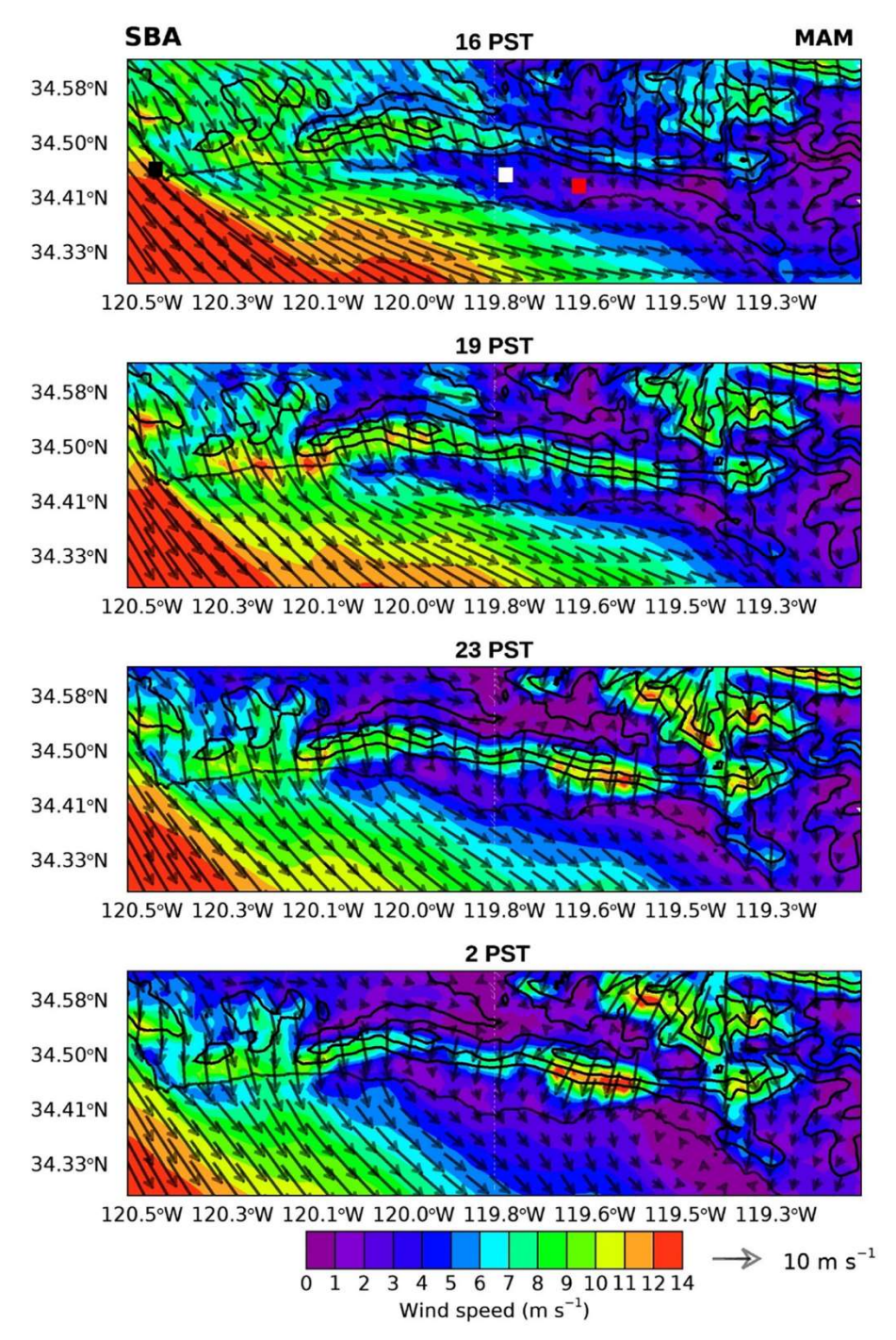


Fig. 9. Same as in Fig. 7, but for Santa Barbara Sundowner winds regime during MAM.

5. Mean sea-level pressure gradients and Sundowner winds regimes

Based on years of experience in forecasting Sundowner winds, the NWS LOX has developed a set of criteria that needs to be met for downslope windstorms to occur in the SYM (Carvalho et al., 2020; Ryan, 1996; Sukup, 2013). The NWS LOX considers a significant Sundowner event when cross-mountain northerly winds have sustained speeds \geq 30 mph (13.4 m s $^{-1}$) and/or gusts \geq 35 mph (15.6 m s $^{-1}$) on the southern slopes of the SYM. The NWS LOX also recognizes that Sundowner winds have distinct characteristics in the western and eastern SYM. As a rule of thumb, the NWS LOX uses mslp differences as forecast guidance: Santa Maria (120.4521 W, 34.8941 N) and Santa

Barbara (119.8403 W, 34.55 N) airports $P_{KSMA-KSBA}$ and Bakersfield (119.0567 W, 35.4336 N) and Santa Barbara $P_{KBFL-KSBA}$ airports.

The mslp synoptic patterns associated with western, eastern and SBA regimes are distinctly different from days without significant downslope winds in the southern slopes of the SYM (Fig. 5) and, therefore, support the forecast guidance used by the NWS LOX. To explore this issue further, we calculated scatterplots and correlations of PC1 and P_{KSMA-KSBA} and PC2 and P_{KBFL-KSBA} (Supplementary Fig. S7). The correlation is slightly less for PC2 x P_{KBFL-KSBA} (correlation 0.51) than for PC1 x P_{KSMA-KSBA} (0.64); both mslp metrics show positive and statistically significant correlations with the time coefficients of Sundowner winds activity (correlations above 0.19 are statistically significant at 5% level). This is additionally supported by reversing the

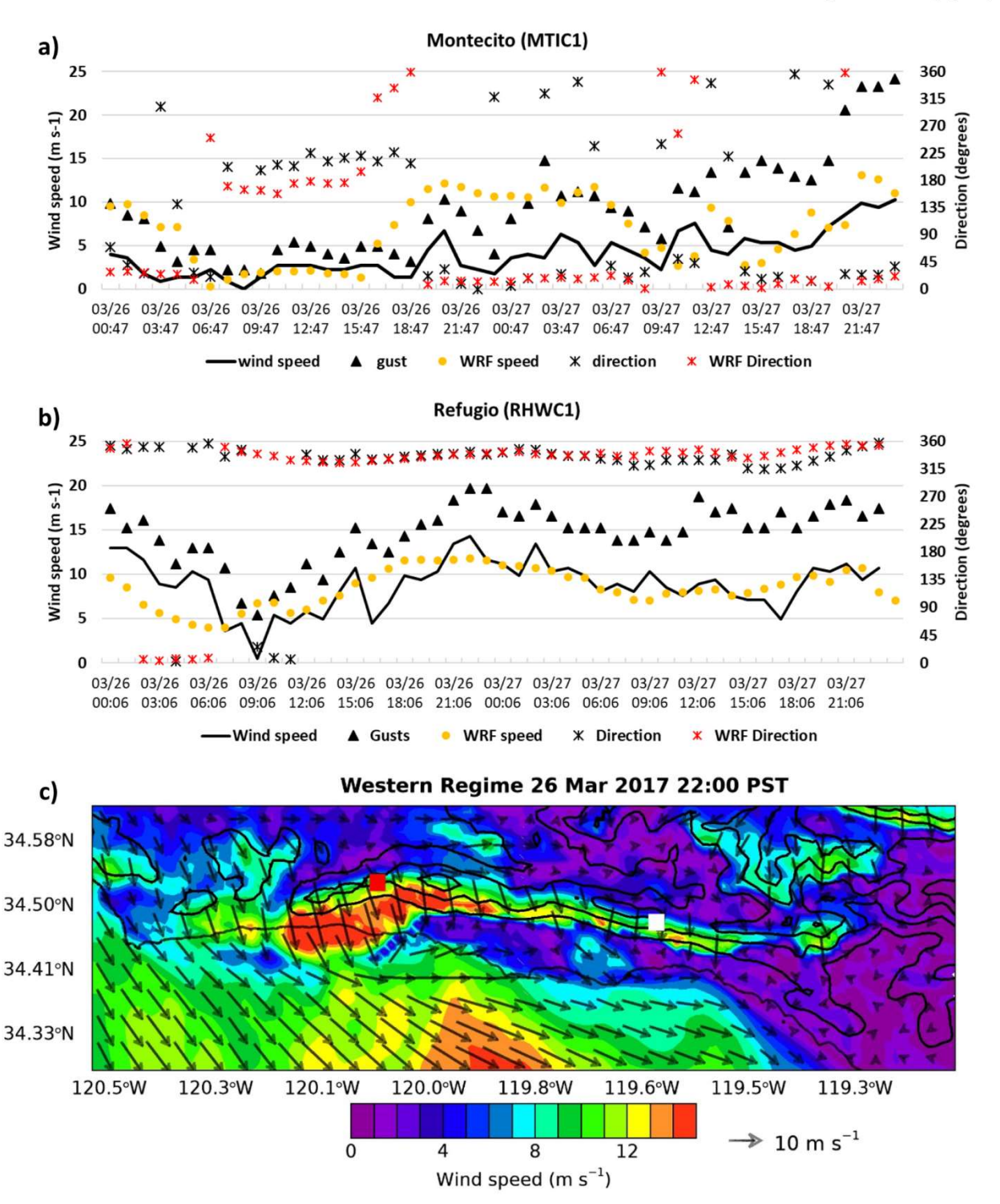


Fig. 10. Sundowner winds in the western regime during 26–27 March 2017. a) and b) show observations of wind speeds (10 m), gusts and direction in the Montecito (white box) and Refugio (red box) stations. WRF wind speeds (10 m) and direction are shown in orange and red symbols. Horizontal axes show local time (PST). c) Simulated WRF winds (10 m) on 26 March 2017 22 PST.

metrics PC2 x $P_{KSMA-KSBA}$ and PC1 x $P_{KBFL-KSBA}$ in which correlations drop to 0.07 and 0.05, respectively. These results support the NWS LOX forecast guidance.

The usefulness of the mslp metrics is further demonstrated with correlations between $P_{KSMA-KSBA},\,P_{KBFL-KSBA}$ and v10 in each grid point (Fig. 15). Negative correlations between $P_{KSMA-KSBA}$ and v10 (Fig. 15a) are observed over most of the domain but are particularly large over the SYM, SRM and over the ocean. Consistent with the NWS LOX forecasters experience, negative correlations between $P_{KBFL-KSBA}$ and v10

(Fig. 15b) are found over the eastern SYM and SRM supporting a different Sundowner regime known locally as Montecito (34.4367 N, 119.6321 W) (i.e., eastern) events.

6. Discussion and conclusions

This study presents a climatology of Sundowner winds using a 30 yr high spatiotemporal downscaling dataset performed with the WRF model (1 km horizontal grid spacing, hourly, 1 September 1987 to 31 $\,$

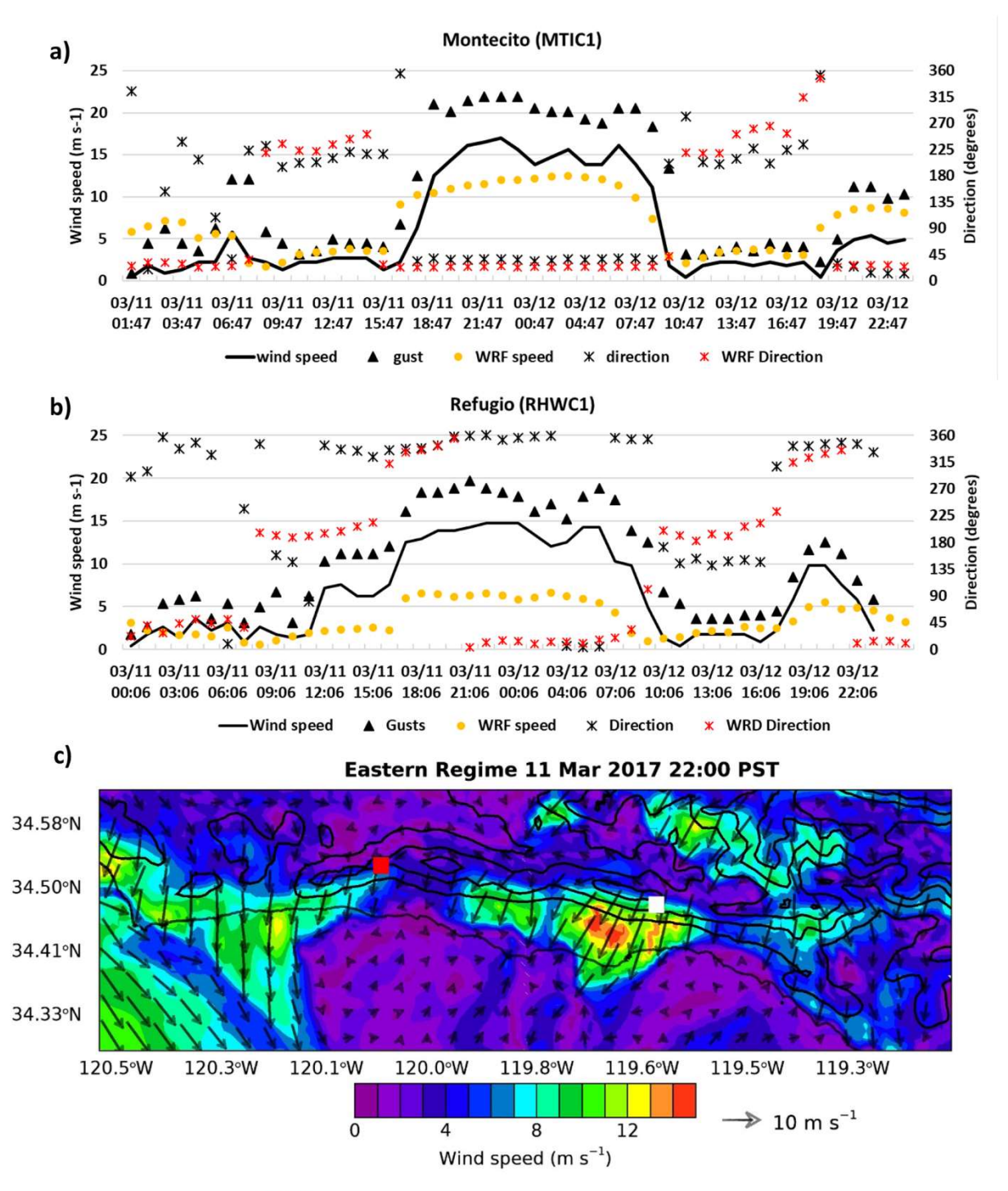


Fig. 11. As in Fig. 10, but for Sundowner winds in the eastern regime during 11–12 March 2017.

August 2017). An objective approach is used to investigate the climatology of Sundowner winds. While other statistical methods such as cluster analysis and self-organizing maps could have been used (e.g., Cavazos et al., 2002; Wilks, 2011), the CEOF method employed here demonstrably characterizes the variability of surface winds. It follows from the mathematical formulation of the CEOF method (Wilks, 2011) that the main modes of surface winds variability are identified naturally from the data without any arbitrary decisions. EOF-1 captures strong surface winds in the western SYM, whereas EOF-2 represents strong downslope winds in the eastern SYM and SRM.

The hourly frequency distributions of the first two time coefficients (PC1, PC2) are used to identify the occurrence of significant downslope

winds on the southern slopes of the SYM. These indices are single time series representing the temporal variability of surface winds and avoid introducing biases due to spatially averaging time series. This aspect is especially important because, as shown here, surface winds, temperature and humidity vary significantly along the SYM and the Santa Barbara coastal plain during Sundowner winds. The hourly percentile thresholds of PC1 and PC2 are the only arbitrary decisions used in our methodology, but these have been tested against historical Sundowner wind events. Evidently, increasing/decreasing thresholds simply identify less/more events and, thus, capture more extreme/mild downslope winds. The definition of Sundowner winds used here is based exclusively on surface winds and does not include adiabatic warming and

Atmospheric Research 249 (2021) 105305

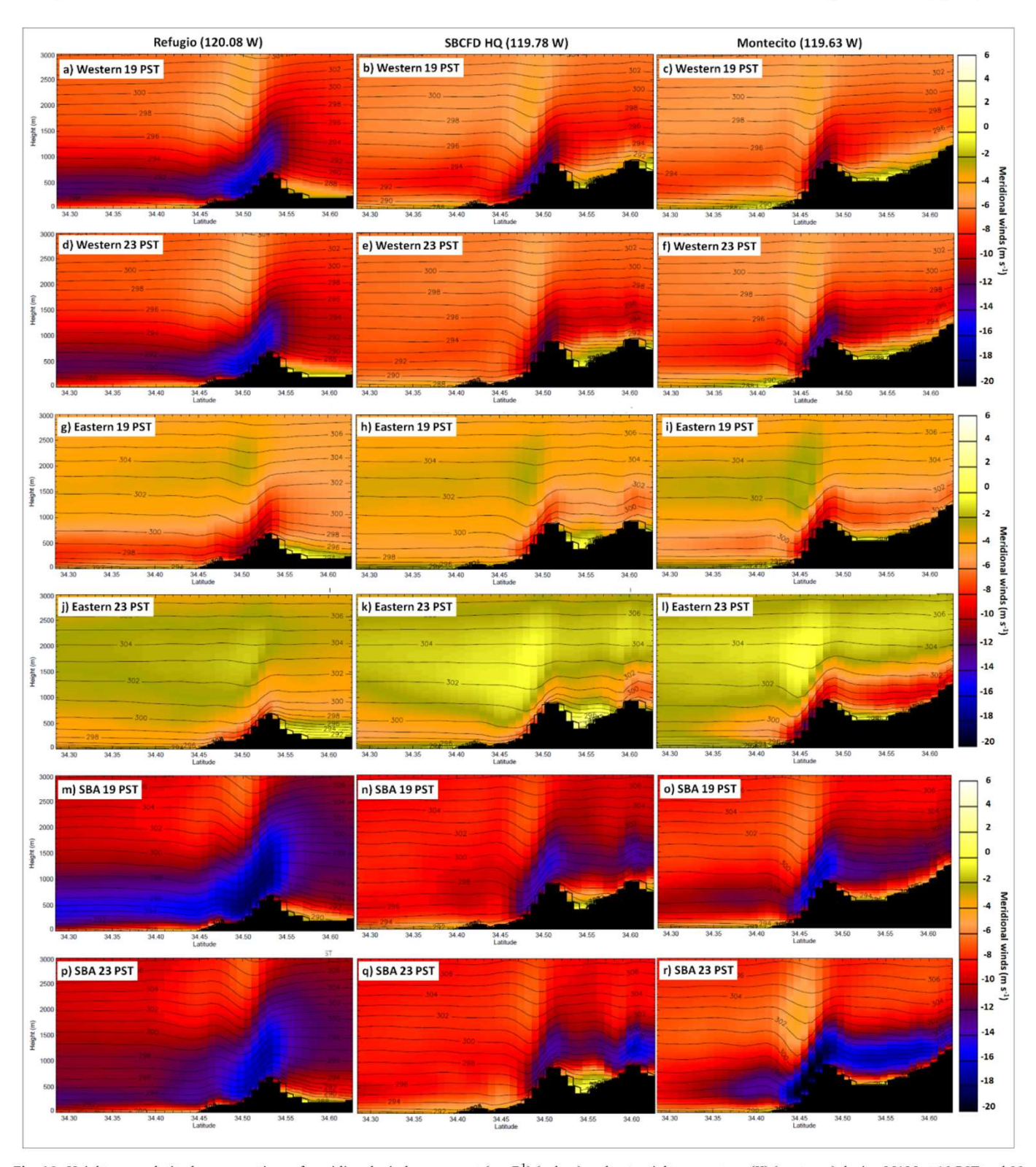


Fig. 12. Height versus latitude cross sections of meridional wind component (m s⁻¹) (colors) and potential temperature (K) (contours) during MAM at 19 PST and 23 PST. Cross sections are at Refugio (120.08 W), San Marcos (119.78 W) and Montecito (119.63 W). Sundowner winds regimes are: western, eastern and SBA. Dark shading indicates topography.

drying effects at the surface. This is intentionally done because there is large seasonal variability from case-to-case in these variables.

Three types of Sundowner wind regimes are identified: western, eastern and SBA. Each regime is associated with a distinct synoptic pattern and they support the mslp metrics used by the NWS LOX. The seasonal distribution shows that the western regime occurs more frequently than the eastern and

SBA regimes and peaks during MAM, minimum in the summer and increases again in late fall. The frequency of eastern regime has maximum in Jan-Feb, minimizes in the summer and increases again in the fall. The SBA regime is less frequent than the western regime but follows a similar seasonal cycle. The onset of strong downslope winds occurs earlier (16–18 PST) in the western SYM than in the eastern SYM (19–20 PST).

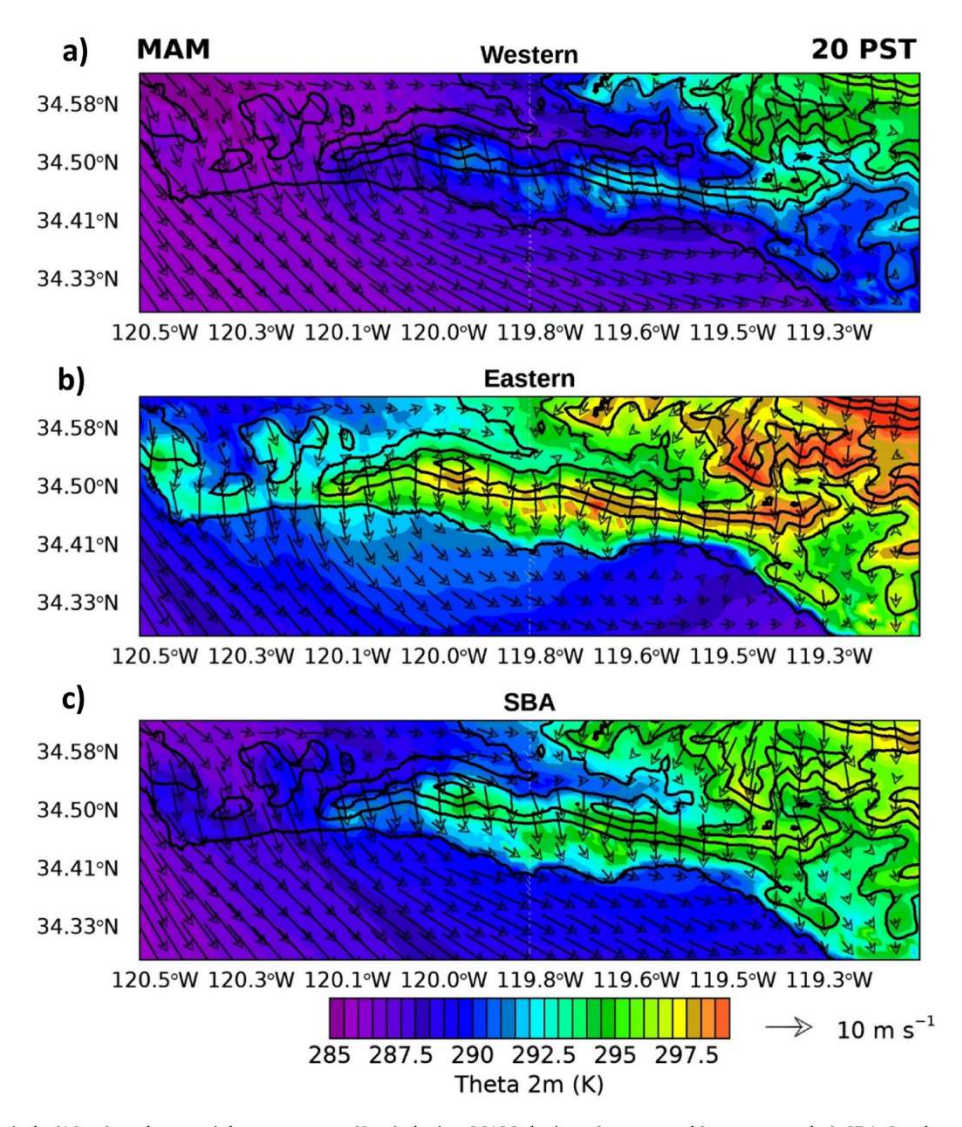


Fig. 13. Composites of winds (10 m) and potential temperature (2 m) during MAM during a) western, b) eastern and c) SBA Sundowner winds regimes. Colors indicate potential temperature (K), vectors show winds and black contours show terrain elevations every 300 m.

In all three regimes, surface winds are strong in the coastal area near Point Conception and western SYM. However, the key difference in the eastern regime is associated with the intensity and direction of the winds in the western SYM. In this situation, surface winds project weakly onto EOF-1, while strong northeasterly downslope winds in the eastern SYM project strongly onto EOF-2. In addition, northwesterly winds are moderate in the Santa Barbara Channel.

The previous studies of Smith et al. (2018a, 2018b) do not recognize the eastern regime (or Montecito) as distinct from the western (or Gaviota) Sundowner events. They used differences in meridional winds and surface temperature relative to a reference location (i.e., La Cumbre Peak 119.7126 W, 34.4944E; 1218 m elevation). To obtain a single index, they spatially averaged the relative differences over a large domain including the coastal plain, western and eastern SYM. Our results show a large degree of spatial variability in which, on average, wind speeds during Sundowner winds range from 1 to 3 m s⁻¹ in some locations in the eastern SYM to more than 14 m s⁻¹ in the western SYM. This implies that the single index of Smith et al. (2018a, 2018b) is heavily skewed by the strong winds in the western SYM and, consequently, is unable to differentiate between strong downslope winds in the western and eastern SYM. Smith et al. (2018b) state that this is a caveat in their methodological approach.

Sundowners show localized areas of strong surface winds along the

slopes and foothills of the SYM with diurnal and seasonal variations. These characteristics of Sundowner winds create different fire weather regimes and fire behavior, which are strongly dependent on vegetation fuels, topography and ignitions as well (Zigner et al., 2020). Although the investigation of Sundowner mechanisms is beyond the scope of this study, our results indicate that western, eastern and SBA Sundowners are driven by distinct synoptic-to-mesoscale processes. Additional investigation is necessary to validate model results as well as understand the interaction among Sundowner winds, upstream atmospheric stability and boundary layer structures in the Santa Ynez Valley and downstream over the ocean from observational and modeling initiatives. These aspects underscore the need to improve the observational network and undertake field campaigns to investigate critical fire weather regimes.

Declaration of Competing Interest

None.

Acknowledgements

This research was supported by the National Science Foundation (Integrative and Collaborative Education and Research, ICER 1664173

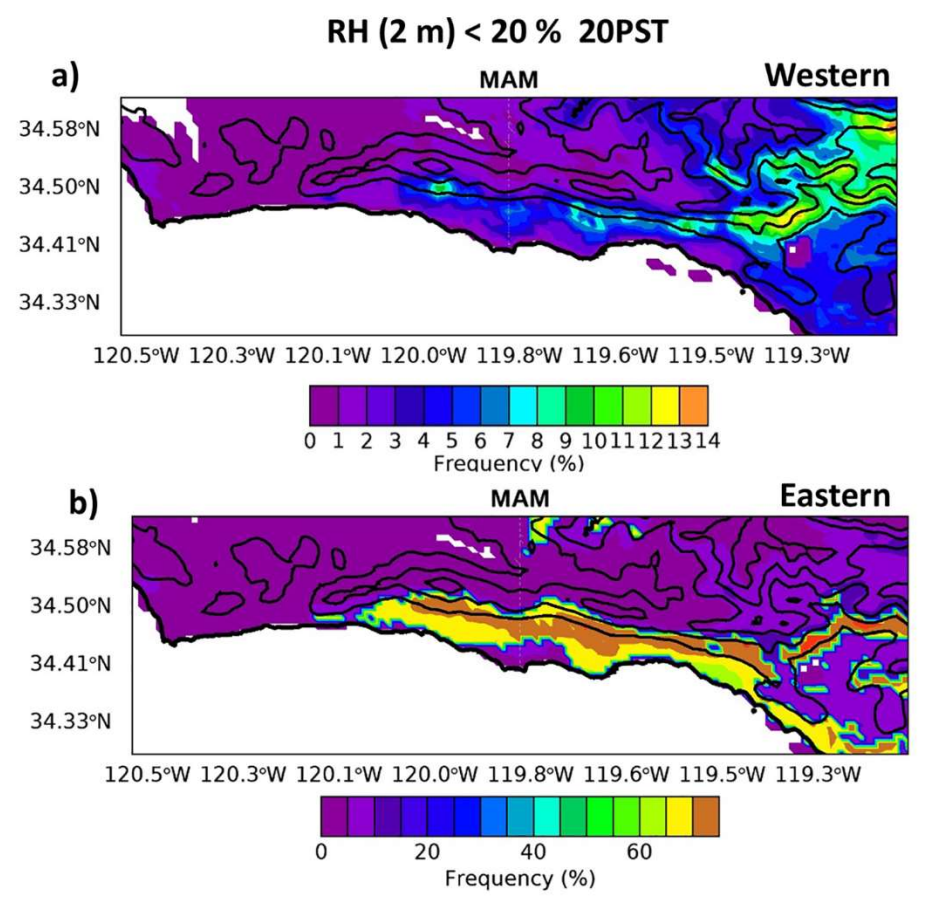


Fig. 14. Frequency of days during MAM when relative humidity (2 m) is less than 20% at 20:00 local time (PST): a) western and b) eastern regimes. Note that scales are different for each regime.

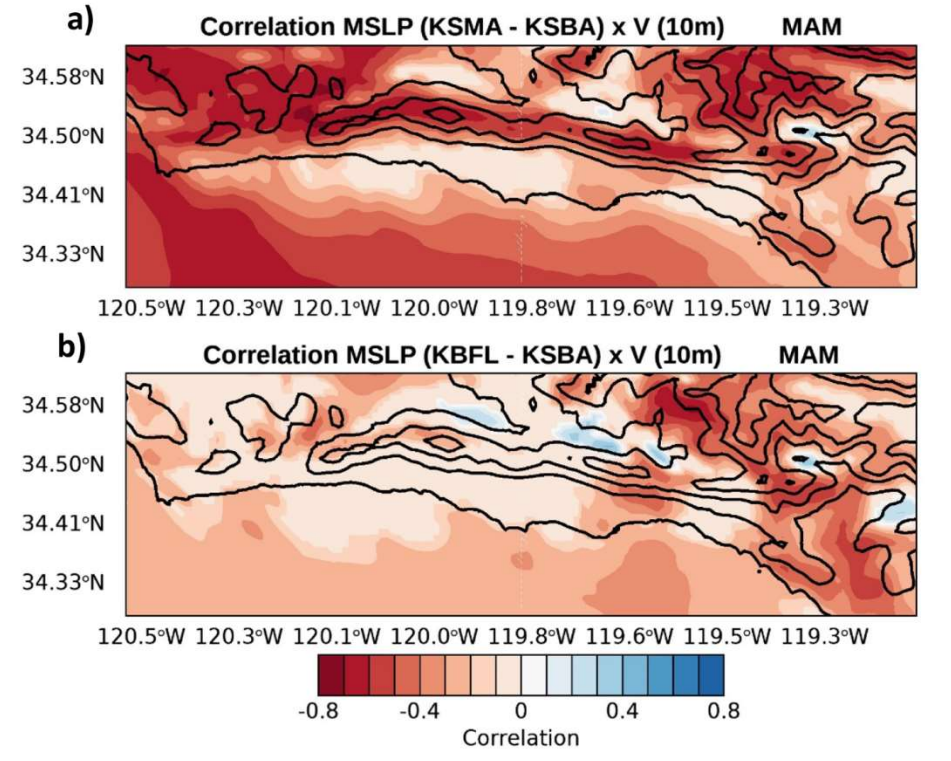


Fig. 15. a) correlations between difference in mean sea level pressure (mslp) in Santa Maria (KSMA) and Santa Barbara (KSBA) airports and meridional wind component (10 m). b) correlations between difference in mean sea level pressure (mslp) in Bakersfield (KBFL) and Santa Barbara (KSBA) airports and meridional wind component (10 m). Correlations are shown for all days and hours in MAM season. Correlations greater (less) than 0.15 (-0.15) are statistically significant at 5% level.

and AGS 1921596) and the University of California Lab Fees Program (LFR-20-652467). We would like to acknowledge high-performance computing support from Cheyenne (doi:https://doi.org/10.5065/D6RX99HX) provided by NCAR's Computational and Information Systems Laboratory, sponsored by the National Science Foundation. The authors thank Jimmy Dudhia (NCAR) for valuable discussions related to WRF and the forecasters from the National Weather Service Los Angeles/Oxnard Office for their support. The support of the Santa Barbara County Fire Department is also appreciated.

Appendix A. Supplementary data

Supplementary data to this article can be found online at https://doi.org/10.1016/j.atmosres.2020.105305.

References

- Blier, W., 1998. The Sundowner Winds of Santa Barbara, California. Weather Forecast. 13, 702–716. https://doi.org/10.1175/1520-0434(1998)013<0702:TSWOSB>2.0.
- Cannon, F., Carvalho, L.M.V., Jones, C., Hall, T., Gomberg, D., Dumas, J., Jackson, M., 2017. WRF simulation of downslope wind events in coastal Santa Barbara County. Atmos. Res. 191, 57–73. https://doi.org/10.1016/j.atmosres.2017.03.010.
- Cao, Y., Fovell, R.G., 2016. Downslope windstorms of San Diego County. Part I: a case study. Mon. Weather Rev. 144, 529–552. https://doi.org/10.1175/Mwr-D-15-0147.1.
- Carvalho, L.M.V., Duine, G.-J., Jones, C., Zigner, K., Clements, C., Kane, H., Gore, C., Bell, G., Gamelin, B., Gomberg, D., Hall, T., Johnson, M., Dumas, J., Boldt, E., Hazard, R., Enos, W., 2020. The Sundowner Winds Experiment (SWEX) Pilot Study: understanding downslope windstorms in the Santa Ynez Mountains, Santa Barbara, CA. Mon. Weather Rev. 148, 1519–1539.
- Cavazos, T., Comrie, A.C., Liverman, D.M., 2002. Intraseasonal variability associated with wet monsoons in Southeast Arizona. J. Clim. 15, 2477–2490.
- Conil, S., Hall, A., 2006. Local regimes of atmospheric variability: a case study of Southern California. J. Clim. 19, 4308–4325. https://doi.org/10.1175/JCLJ3837.1.
- Dee, D.P., Uppala, S.M., Simmons, A.J., Berrisford, P., Poli, P., Kobayashi, S., Andrae, U., Balmaseda, M.A., Balsamo, G., Bauer, P., Bechtold, P., Beljaars, A.C.M., van de Berg, L., Bidlot, J., Bormann, N., Delsol, C., Dragani, R., Fuentes, M., Geer, A.J., Haimberger, L., Healy, S.B., Hersbach, H., Hólm, E.V., Isaksen, L., Kållberg, P., Köhler, M., Matricardi, M., McNally, A.P., Monge-Sanz, B.M., Morcrette, J.-J., Park, B.-K., Peubey, C., de Rosnay, P., Tavolato, C., Thépaut, J.-N., Vitart, F., 2011. The ERA-Interim reanalysis: configuration and performance of the data assimilation system. Q. J. R. Meteorol. Soc. 137, 553–597. https://doi.org/10.1002/qj.828.
- Dorman, C.E., Koračin, D., 2008. Response of the summer marine layer flow to an extreme California Coastal Bend. Mon. Weather Rev. 136, 2894–2992. https://doi.org/10. 1175/2007/MWR2336.1
- Doubler, D.L., Winkler, J.A., Bian, X., Walters, C.K., Zhong, S., 2015. An NARR-derived climatology of Southerly and Northerly low-level jets over North America and Coastal Environs. J. Appl. Meteorol. Climatol. 54, 1596–1619. https://doi.org/10.1175/ JAMC-D-14-0311.1.
- Duine, G.-J., Jones, C., Carvalho, L., Fovell, R., Duine, G.-J., Jones, C., Carvalho, L.M.V., Fovell, R.G., 2019. Simulating Sundowner Winds in Coastal Santa Barbara: model validation and sensitivity. Atmosphere (Basel) 10, 155. https://doi.org/10.3390/ atmos10030155.
- Durran, D.R., 1990. Mountain waves and downslope winds. Atmos. Process. Complex Terrain 23, 59–81.
- Hatchett, B.J., Smith, C.M., Nauslar, N.J., Kaplan, M.L., 2018. Brief communication:

- synoptic-scale differences between Sundowner and Santa Ana wind regimes in the Santa Ynez Mountains, California. Nat. Hazards Earth Syst. Sci. 18, 419–427. https://doi.org/10.5194/nhess-18-419-2018.
- Hong, S.-Y., Lim, J.-O.J., 2006. The WRF single-moment 6-class microphysics scheme (WSM6). J. Korean Meteorol. Soc. 42, 129–151.
- Hughes, M., Hall, A., 2009. Local and synoptic mechanisms causing Southern California's Santa Ana winds. Clim. Dyn. 34, 847–857.
- Iacono, M.J., Delamere, J.S., Mlawer, E.J., Shephard, M.W., Clough, S.A., Collins, W.D., 2008. Radiative forcing by long-lived greenhouse gases: Calculations with the AER radiative transfer models. J. Geophys. Res. 113https://doi.org/10.1029/ 2008jd009944. doi:Artn D13103Doi.
- Jones, C., Carvalho, L.M.V., 2012. Spatial-intensity variations in extreme precipitation in the contiguous United States and the Madden-Julian Oscillation. J. Clim. 25, 4898–4913. https://doi.org/10.1175/jcli-d-11-00278.1.
- Jones, C., Fujioka, F., Carvalho, L.M.V., 2010. Forecast skills of synoptic conditions associated with Santa Ana winds in southern California. Mon. Weather Rev. 138, 4528–4541. https://doi.org/10.1175/2010MWR3406.1.
- Kolden, C., Abatzoglou, J., 2018. Spatial distribution of wildfires ignited under Katabatic versus Non-Katabatic Winds in Mediterranean Southern California USA. Fire 1, 19. https://doi.org/10.3390/fire1020019.
- Ludwig, F.L., Horel, J., Whiteman, C.D., 2004. Using EOF analysis to identify important surface wind patterns in mountain valleys. J. Appl. Meteorol. 43, 969–983. https:// doi.org/10.1175/1520-0450(2004)043 < 0969:UEATII > 2.0.CO;2.
- Moritz, M.A., Moody, T.J., Krawchuk, M.A., Hughes, M., Hall, A., 2010. Spatial variation in extreme winds predicts large wildfire locations in chaparral ecosystems. Geophys. Res. Lett. 37, L04801.
- Nakanishi, M., Niino, H., 2009. Development of an improved turbulence closure model for the atmospheric boundary layer. J. Meteorol. Soc. Japan. Ser. II 87, 895–912. https://doi.org/10.2151/jmsj.87.895.
- Niu, G.Y., Yang, Z.L., Mitchell, K.E., Chen, F., Ek, M.B., Barlage, M., Kumar, A., Manning, K., Niyogi, D., Rosero, E., Tewari, M., Xia, Y., 2011. The community Noah land surface model with multiparameterization options (Noah-MP): 1. Model description and evaluation with local-scale measurements. J. Geophys. Res. Atmos. 116. https://doi.org/10.1029/2010JD015139.
- North, G.R., Bell, T.L., Cahalan, R.F., Moeng, F.J., 1982. Sampling errors in the estimation of empirical orthogonal functions. Mon. Weather Rev. 110, 699–706.
- Olson, J.B., Kenyon, J.S., Angevine, W.A., 2019. A Description of the MYNN-EDMF Scheme and the Coupling to Other Components in WRF-ARW. https://doi.org/10. 25923/n9wm-be49.
- Raphael, M.N., 2003. The Santa Ana Winds of California. Earth Interact. 7, 1–13. Ryan, G., 1996. Downslope winds of Santa Barbara, California. NWS WR-240. In: National Weather Service Western Region, Oxnard, California.
- Skamarock, W.C., Klemp, J.B., Dudhia, J., Gill, D.O., Barker, D.M., Duda, M.G., Huang, X.-Y., Wang, W., Powers, J.G., 2008. A Description of the Advanced Research WRF Version 3. NCAR/TN-475+STR, NCAR Technical Note. (113 pp).
- Smith, C.M., Hatchett, B., Kaplan, M., 2018a. Characteristics of Sundowner Winds near Santa Barbara, CA, from a dynamically downscaled climatology: environment and effects aloft and offshore. J. Geophys. Res. Atmos. 123. https://doi.org/10.1029/ 2018JD029065.
- Smith, C.M., Hatchett, B.J., Kaplan, M.L., 2018b. Characteristics of Sundowner winds near Santa Barbara, California, from a dynamically downscaled climatology: environment and effects near the surface. J. Appl. Meteorol. Climatol. 57, 589–606. https://doi.org/10.1175/Jamc-D-17-0162.1.
- Sukup, S., 2013. Extreme northeasterly wind events in the hills above Montecito, California. In: Western Region Technical Attachment NWS WR-1302, National Weather Service Western Region, Salt Lake City, UT.
- Wilks, D.S., 2011. Statistical Methods in the Atmospheric Sciences, Second ed. Academic Press, Inc, San Diego, California, USA.
- Zigner, K., Carvalho, L.M.V., Peterson, S., Fujioka, F., Duine, G.-J., Jones, C., Roberts, D., Moritz, M., 2020. Evaluating the ability of FARSITE to simulate wildfires influenced by extreme, downslope winds in Santa Barbara, California. Fire 3, 29. https://doi. org/10.3390/fire3030029.